ELSEVIER

Surface and Coatings Technology 142–144 (2001) 110–116

SURFACE & COATINGS TECHNOLOGY

www.elsevier.com/locate/surfcoat

Elastic properties of (Ti,Al,Si)N nanocomposite films

S. Carvalho[a,*], F. Vaz[a], L. Rebouta[a], D. Schneider[b], A. Cavaleiro[c], E. Alves[d]

[a] *Physics Department, University of Minho, Azurém, 4810 Guimarães, Portugal*
[b] *Fraunhofer Institut für Werkstoffphysik, Dresden, Germany*
[c] *ICMES-FCT, University of Coimbra, 3030 Coimbra, Portugal*
[d] *ITN, Physics Department E.N.10, 2686-953 Sacavém, Portugal*

Abstract

(Ti,Al,Si)N films have been prepared by d.c. and rf reactive magnetron sputtering, with Si contents in the range 2–11 at.% and Al contents between 4 and 19 at.%. Samples prepared in rotation mode (three magnetrons) presented densities between 4.0 and 4.6 g/cm^3, while samples prepared in static mode (magnetron with Ti target with small pieces of Si and Al) displayed densities mainly in the range 3.0–3.9 g/cm^3. For comparison purposes, the evaluation of Young's modulus was performed by both depth-sensing indentation and surface acoustic wave (SAW) techniques. Indentation results revealed systematically higher values than those obtained by SAW. These discrepancies might be related with the relatively low density of the films. Hardness values of approximately 60 GPa were obtained with samples with a composition of approximately 28.5 at.% titanium, 12 at.% aluminium, 9.5 at.% silicon and 50 at.% nitrogen. XRD patterns showed the presence of two different crystalline phases, as in the case of (Ti,Si)N films. One is assigned to TiN phase (lattice parameter of approx. 0.429 nm) and the second, the so-called solid solution which is developed in situations of low surface mobility, revealed a lattice parameter (0.419 nm) slightly lower than that of bulk TiN.

Keywords: Superhard coatings; Young's modulus; Ti–Al–Si–N; Elastic modulus

1. Introduction

In the field of thin films, engineering solutions for several technological problems depend on the capacity to measure physical and mechanical properties of films [1]. Elastic modulus (Young's modulus) of nanocomposite films is one of the most important mechanical properties and it is of prime importance in applied and fundamental research. This parameter represents the stiffness of the material that correlates with the atomic structure [2], since variations in Young's modulus reflect changes in crystallinity, orientation and quality of thin films [3], as well as providing information about propagation of cracks and pores [4].

Tabulated Young's modulus values from bulk material often deviate far from those realised in films of the same materials. For several film materials, bulk properties are not known since they cannot be obtained as bulk samples [2]. Therefore a wide variety of methods have been studied and developed in order to measure the elastic properties of thin films [5,6]. Interest in indentation of films has been gaining increasing importance with the development of very low load depth-sensing indentation instruments [7,8], which allow one to make indentations as shallow as a few nanometres [9]. The stiffness of the contact between the indenter tip and the material is then relatively small and can be measured accurately as required for reliable hardness and Young's modulus measurements [10]. Laser acoustic techniques also allow the Young's modulus determination [11,12]. These techniques are based on the measurement of the dispersion of surface acoustic waves that are generated by short laser pulses.

This paper reports on the Young's modulus of (Ti,Al,Si)N coatings, deposited by reactive magnetron

* Corresponding author.

0257-8972/01/$ - see front matter
PII: S0257-8972(01)01242-7

sputtering, obtained by indentation and SAW techniques. (Ti,Al)N already demonstrated significant improvements in hardness and heat resistance over conventional binary metal nitrides [13–17]. The main objective of this work was to study the influence of Si addition to (Ti,Al)N matrix and obtain (Ti,Al,Si)N coatings with improved oxidation resistance [18,19] when compared with that of (Ti,Si)N films and with the same high hardness and elasticity [20–26]. Correlation between Young's modulus and some deposition parameters, as well as its correlation with density, will be analysed in some detail.

2. Experimental details

2.1. Sample preparation

For this study (Ti,Al,Si)N thin coatings were deposited by rf and d.c. reactive magnetron sputtering in an Ar/N_2 atmosphere, on high-speed steel (M2) and single crystal silicon (100) substrates. The substrates were cleaned by pre-sputtering (etching) during 10 min in an Ar atmosphere with 200 W rf power supply.

Two series of samples were produced in rotation mode, from high-purity Ti, Si, Al targets, with a constant substrate holder rotation of 4 rev./min. In this mode, the experiments were carried out with the Silicon target coupled to a rf source (1.3–3.1 W/cm^2), and aluminium target coupled to a d.c. source (1.5–2.6 mA/cm^2). Some samples were prepared with a titanium target coupled to a rf source (3.1–4.0 W/cm^2), while others were deposited using a d.c. power supply (6.4 mA/cm^2). A Ti adhesion layer of approximately 0.35 μm was deposited onto these samples before coating deposition. A third series of samples was produced in static mode with some pieces of Si and Al (with known area) on titanium target, which was coupled to a rf power supply (using a power density of 2.6 and 3.7 W/cm^2).

The substrates were heated for temperatures ranging from 200 to 500°C and d.c. biased from -100 to -25 V. A target to substrate distance of 60 mm was kept constant in all runs. The sputtering chamber was evacuated with a turbomolecular pump down to a base vacuum pressure less than 2×10^{-4} Pa. During depositions the working pressure was approximately 0.5 Pa. The Argon flow was kept constant at 100 sccm while the N_2 flow was varied from 2 to 5 sccm in order to obtain a nitrogen content on samples of approximately 50 at.%.

After depositions, the samples were analysed by X-ray-diffraction (XRD), in a Philips PW 1710 apparatus using Cu K_α radiation. The composition was analysed by electron microprobe analysis (EMPA) and Rutherford backscattering spectrometry (RBS). In order to extract the areal atomic density, a proton beam of 1.6 MeV was used in RBS experiments. Film thickness was obtained by ball cratering.

2.2. Depth-sensing indentation

Indentation experiments were performed in a computer-controlled Fischerscope H100 ultramicrohardness tester, equipped with a Vickers diamond indenter. During testing, the load is incremented continuously during both loading and unloading. The slope of the upper portion of the unloading curve can be used as a measure of the Young's modulus of the sample. If the area in contact remains constant during initial unloading, the elastic behaviour may be modelled as that of a blunt punch indenting an elastic solid. Young's modulus can be calculated by the slope of the initial portion of the unloading curve, by adopting Sneddon's flat-ended cylinder punch model [27]. By equating the projected area in contact under the indenter to the punch area and putting the equation in the form of unloading slope, one obtains for a Vickers indenter [28,29]:

$$S^{-1}=\frac{dh}{dP}=\frac{1}{2h_p}\left(\frac{\pi}{24.5}\right)^{1/2}\cdot\left(\frac{1}{E_r}\right) \quad (1)$$

where $1/E_r=(1-\nu_f^2)/E_f+(1-\nu_i^2)/E_i$, with E_f and ν_f being the Young's modulus and Poisson's ratio for the film ($\nu_f=0.25$) and E_i and ν_i, the same quantities for the diamond indenter ($E_i=1141$ GPa and $\nu_i=0.07$ [30]). The term h_p is the plastic depth that can be obtained from the load–displacement curve. This method and these equations assume that during initial unloading the area in contact with the indenter remains constant, and that the indenter has an ideal pyramidal geometry. Nevertheless, some corrections regarding the imperfections of the diamond indenter have to be considered — the so-called indenter offset. For the equipment used in this work, the expression $h_{corr}=0.052+1.095h_p$ is used to correct the indentation depth [31]. When using the ultramicrohardness tester with thin coatings (2 μm), a further factor has to be considered in order to avoid the influence of the substrate on the measured values. The criterion $h_{max}<0.1t$ (t is the coating thickness) is well accepted as the condition that guarantees that the substrate influence is avoided [32]. It is frequently observed that as the load is decreased in indentation experiments, the apparent hardness of the surface increases — the so-called indentation size effect (ISE) [33]. This effect can be the result of material pileup around the indenter, or the result of incorrect calibration of the indenter area function. Another factor that can affect the apparent ISE is the magnitude of the thermal drift correction. In certain instrument configurations these corrections can be significant, particularly at low loads. The data from

the hold segment (30 s) at the last unloading stage were used to correct the load–unload displacement data for thermal drift [25].

In order to avoid the influence of the substrate, a maximum load of 40 mN was used in measurements, although in some cases a maximum load of 60 mN was applied.

2.3. Laser–acoustic method

Surface acoustic waves (SAW) propagate along the surface of a material. Their amplitude decays exponentially perpendicular to the surface. The decays length is approximately equal to the wavelength λ [34], leading to a penetration depth decrease with increasing frequency. The interesting wave parameter is the propagation velocity, which is related to Young's modulus. In a system coating/substrate the propagation velocity (c) is dependent on frequency, which is called dispersion. This is attributable to the fact that surface waves with different frequencies have different depths of penetration and are influenced differently by the properties coating/substrate system [3,35]. Those parameters are the following seven parameters of the substrate and the film material: Young's moduli E_s and E_f, densities ρ_s and ρ_f, Poisson's ratio ν_s and ν_f and film thickness (t). So, the dispersion relation in a general form can describe the correlation between sound propagation velocity and material parameters;

$$c = \frac{\overline{\omega}}{k} = c\left(\frac{t}{\lambda}, E_f, E_s, \rho_f, \rho_s, \nu_f, \nu_s\right) \tag{2}$$

where $\omega = 2\pi f$ is the circular frequency and $k = 2\pi/\lambda$ is the wave number.

The measurement of the dispersion curve (phase velocity vs. frequency) requires that the surface waves have to be generated and detected in a wide frequency range. A short laser pulse of the nitrogen laser is applied for generating wide band surface wave impulses. A cylindrical lens focuses the beam onto the specimen surface. The short-time local heating within the laser focus line launches the acoustic impulse, which in turn propagates over the surface of the test piece. The impulse is detected by a wide-band piezoelectric transducer [36] fixed on the sample surface at a distance (x) of some millimetres from the laser focus line. The surface acoustic waveform is detected at different distances (x_1, x_1', x_2) between laser focus line and transducer and recorded on an oscilloscope. An example of the signals detected at different distances with a (Ti,Al,Si)N sample is shown in Fig. 1. The signals detected at x_1, x_1' and x_2 have different forms, showing a decrease in amplitude and a broadening with the distance from the focus line. This phenomenon is caused by the surface wave dispersion. As was refereed earlier, the influence of the film on the surface wave propagation increases with an increase in frequency. The surface wave impulse can be regarded as consisting of an additive superposition of elastic waves of different frequencies. Since every wave component propagates with its own velocity, the impulse is deformed as it travels along its path. Fourier transform of the waveforms yields their phase spectra [11], which enables the calculation of phase velocity as a function of frequency (experimental dispersion curve — $c(f_i)$).

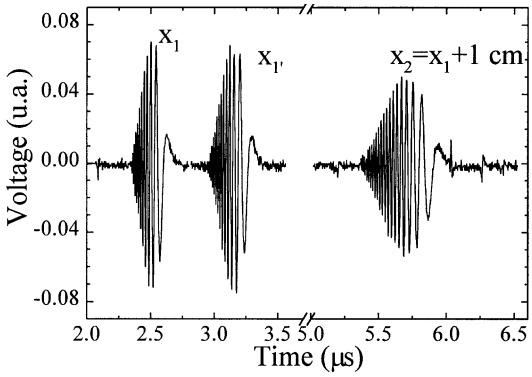

Fig. 1. Surface wave impulses detected on high-speed steel with (Ti,Al,Si)N film at different distances between the laser focus line and detector.

The experimental dispersion curve is fitted to obtain the film parameters making use of the well-known least square method, which can be formulated as follows:

$$\sum_i \left[c(f_i) - c\left(\frac{t}{\lambda}, E_f, E_s, \rho_f, \rho_s \nu_f, \nu_s\right)\right]^2 \to \min \tag{3}$$

in which $c(f_i)$ are the values of surface wave velocity measured for a series of frequencies f_i, and $c(t/\lambda, E_f, E_s, \rho_f, \rho_s, \nu_f, \nu_s)$ are the values calculated from Eq. (2) which is derived from the boundary conditions [37].

The fit yields Young's modulus of the film and also of the substrate (E_f, E_s). The number of material parameters that can be obtained depends on the film thickness, the substrate material and on the bandwidth of the measurement. In the present case only one parameter of the film material could be obtained (e.g. Young's modulus) for the (Ti,Al,Si)N on steel. The density and the thickness of the film material had to be inserted into the fitting procedure. In the case of the films on (100) silicon substrate Young's modulus (E') and the density (ρ') were calculated by the fitting procedure due the large bandwidth, like we can see on measured and fitted curves for (Ti,Al,Si)N on steel and silicon presented in Fig. 2. These fits yield a density of 4.0 g/cm^3 and Young's modulus of 222 and 238 GPa for the same coating deposited on silicon and high-speed steel, respectively. The narrower bandwidth (5 MHz $< f <$ 75 MHz) obtained in the (Ti,Si,Al)N coated

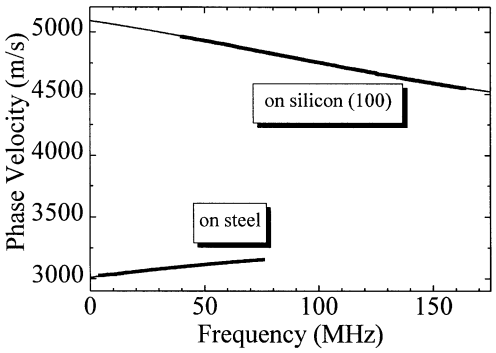

Fig. 2. Surface wave velocity vs. frequency measured on (Ti,Al,Si)N film deposited on high-speed steel and (100) silicon substrates.

steel substrate is caused by the higher ultrasonic attenuation at high frequency waves when compared with (Ti,Si,Al)N coated silicon substrate (40 MHz $< f <$ 160 MHz).

The error of the fit results depends on the number of the fitted parameters and the uncertainty of the input parameters [38]. Inserting the density (ρ) and thickness (t) as input parameters, the uncertainty is given by:

$$\frac{\Delta E}{E} = \frac{\Delta \rho}{\rho} + \frac{\Delta t}{t} \tag{4}$$

which can reach a value of approximately 20%.

3. Results and discussion

3.1. Chemical analysis and density

(Ti,Al,Si)N coatings were deposited with different deposition rates, ranging between 0.3 and 1.3 μm/h. The Ti composition of the as deposited samples varied between 20 and 42.5 at.%, and the Al composition changed from 4 to 19.0 at.%. The silicon contents ranged from 2 to 11 at.% and the nitrogen contents are within the range 47–53 at.%.

The density of the coatings was estimated using the areal atomic density, extracted from RBS measurements, divided by the thickness measured by ball cratering. The uncertainty is approximately 15%, due to the thickness measurement (five tests) and to the averaged error in stopping power used in RBS fitting procedure.

Samples prepared in rotation mode (three magnetrons) presented densities between 4.0 and 4.6 g/cm^3, while those prepared in static mode (one magnetron) revealed densities mainly in the range 3.0–3.9 g/cm^3. These values are much lower than that of bulk TiN (5.4 g/cm^3), but comparable with $Ti_{0.5}Al_{0.5}N$ theoretical density (4.54 g/cm^3), which might be understandable, since in most of the coatings the total amount of Al + Si is approximately 20 at.%. The change in substrate temperature during deposition (300–500°C) did not induce significant changes in density, as well the changes in bias voltage (from −25 to −100 V).

3.2. Texture

XRD patterns showed the presence of two different crystalline phases, as exemplified in Fig. 3. These patterns were obtained with samples with contents of approximately 28.5 at.% titanium, 12 at.% aluminium, 9.5 at.% silicon and 50 at.% nitrogen. These samples were prepared with a substrate temperature of 400°C. The development of these two structures, which are similar to the TiN one, is strongly related with deposition parameters and the respective adatom surface mobility. The phase noted as phase 2, with a lattice parameter (0.419 nm) slightly lower than that of bulk TiN (0.424 nm), develops in situations of low surface mobility (Fig. 3a). This phase was also present in (Ti,Si)N coatings in cases of low substrate temperature and/or low ion bombardment, and was identified as a solid solution with a fcc structure where the Si atom substitutes some of the Ti positions [39,40].

The phase noted as phase 1 with a lattice parameter (0.429 nm) greater than the TiN bulk one, is developed only in conditions of intense ion bombardment. This behaviour can be associated with the segregation of the SiN_x phase and the formation of TiN nanocrystals,

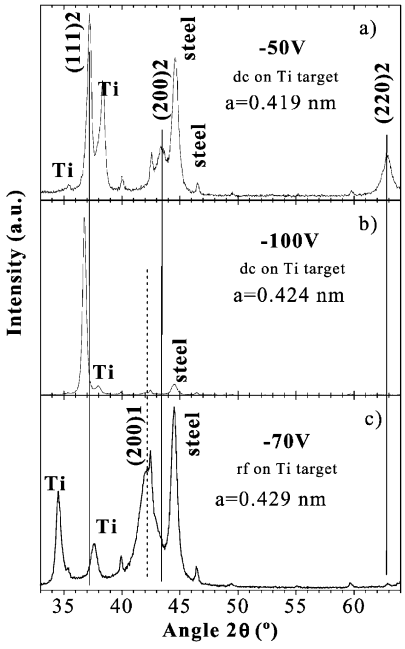

Fig. 3. XRD patterns of samples prepared in rotation mode with a substrate temperature of 400°C. The composition of these samples is approximately 28.5 at.% titanium, 12 at.% aluminium, 9.5 at.% silicon and 50 at.% nitrogen. In the spectra the Ti peaks show the growth of the Ti adhesion layer.

justifying the decrease in the grain size and thus, phase 1 can be assigned to a bulk TiN phase (Fig. 3c). The segregation of SiN_x is not evident, but this is a behaviour that agrees with chemical behaviour of metallic elements, the changes in microstructure and mechanical properties with increasing surface mobility during preparation, as also described for (Ti,Si)N films. The decrease of grain size seems evident from the peak width of X-ray diffractograms (Fig. 3c). However, similar results were obtained with (Ti,Si)N, which are also supported by TEM analysis and reported in Vaz and co-workers [39,40]. The possible formation of an amorphous AlN phase cannot be excluded, since with an aluminium contents of 12 at.% and with Al atoms substituting Ti atoms in the TiN matrix, a lower lattice parameter should be measured [13]. Phase 1 was developed only when the Ti target was supplied with a rf power supply. In these cases, the density bias current is between three and five times higher than that obtained in the cases of d.c. power supply and for the same deposition rate.

For intermediate levels of adatom surface mobility, textures with an intermediate lattice parameter (0.424 nm) were obtained (Fig. 3b). The reason for this behaviour is not yet identified, but the relatively high residual stresses could be responsible for these deviations associated with the presence of Al, since the lattice parameter of (Ti,Al)N coatings decreases with Al content [13], however a solid solution with both phases could also be possible.

3.3. Elastic modulus

Young's modulus of the substrates (high speed steel) was measured by both techniques. SAW analyses, using a density of 8.56 g/cm^3 and a Poisson ratio of 0.27, resulted in a Young's modulus of 220 GPa, while the indentation technique gave a value of 268 GPa. The reason for this difference is not yet known.

In the calculation of Young's modulus by laser acoustic technique, the film thickness measured by ball cratering and the Poisson's ratio of 0.20 taken from the literature were inserted in the fitting procedure [41]. For samples deposited on steel, the fitting calculation could only be carried out with two free parameters, the Young's moduli of the coating and substrate. Thus, it was also necessary to insert the density calculated from the areal atomic density determined by RBS. Comparative studies to determine the Young's modulus of (Ti,Al,Si)N coatings deposited on steel were performed by indentation and laser acoustic techniques and displayed in Figs. 4 and 5, as a function of bias voltage and substrate temperature, respectively. Fig. 4 shows the results for samples prepared by rotation mode with a substrate temperature of 400°C (solid symbols) and with approximately 9 at.% Si and 12 at.% Al, and by

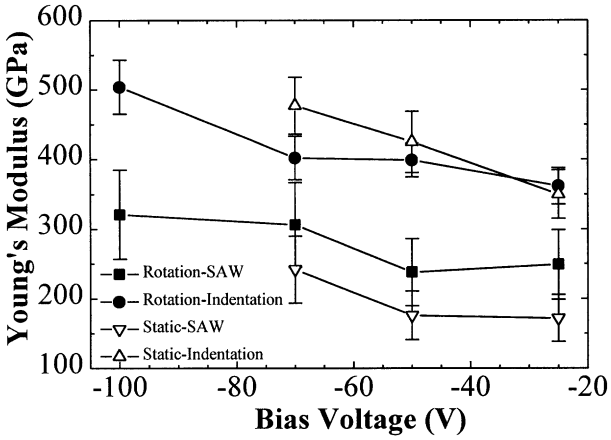

Fig. 4. Young's moduli of the (Ti,Al,Si)N samples as a function of bias voltage, measured by SAW and indentation techniques. The samples prepared by rotation mode (solid symbols) have contents of approximately 9 at.% Si and 12 at.% Al, and those prepared by static mode (open symbols) have contents of approximately 9 at.% Si and 10 at.% Al.

static mode with a substrate temperature of 300°C (open symbols) and with approximately 9 at.% Si and 10 at.% Al. Fig. 5 displays the results for samples prepared by rotation mode (solid symbols) and with approximately 10 at.% Si and 13.5 at.% Al, and by static mode (open symbols) and with approximately 8 at.% Si and 10 at.% Al. This group of samples was prepared with a bias voltage of −50 V. The measurements carried out by SAW were found to be systematically lower than those obtained by indentation. Concerning the elastic modulus measured by SAW technique, the samples prepared by rotation mode presented higher elastic modulus, although those measured by indentation are more similar. Maybe the evolution of the elastic modulus vs. deposition parameters (bias voltage and substrate temperature) is not similar when comparing the results by both methods. However, there is a trend of increasing the elastic modulus with increasing surface mobility that can be well elucidated in Fig. 4.

The big difference in some cases cannot be only explained by possible errors in thickness measurement or in the density evaluation in the case of SAW technique or due to the uncertainty in indentation measurement. The wider frequency range displayed by dispersion curves of samples deposited on silicon (see Fig. 2) allowed the use of a third free parameter in the fitting procedure, the density of the coating. Therefore, SAW analysis of (Ti,Al,Si)N films deposited on silicon wafers allowed the simultaneous calculation of Young's modulus and density of the films. These densities showed a good agreement with those films deposited on steel, and determined by RBS. In order to understand these differences, the Young's modulus was plotted as

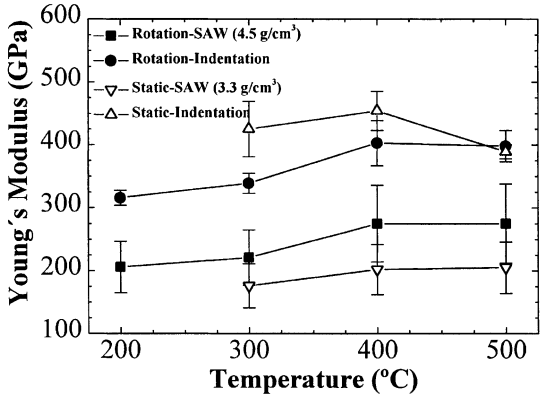

Fig. 5. Young's moduli of the (Ti,Al,Si)N samples as a function of substrate temperature, measured by SAW and indentation techniques. The samples prepared by rotation mode (solid symbols) have contents of approximately 10 at.% Si and 13.5 at.% Al, and those prepared by static mode (open symbols) approximately 8 at.% Si and 10 at.% Al. This group of samples was prepared with a bias voltage of −50 V.

a function of density (Fig. 6). These results show that there is a correlation between the results obtained by SAW and density, revealing an increase in Young's modulus with density. A similar variation using SAW technique was reported by other authors, for ZrO_2 coatings [4], DLC coatings [2] and a-Si:H films [12]. This behaviour is understandable, since elastic modulus describes the stiffness and rigidity of the material, and it is directly related to the density of chemical bonds and their strength. Anyway, the Young's modulus measured by indentation does not show any correlation with density. Thus, it seems that for these films the elastic modulus measured by indentation is not very sensitive to the porosity, which will be related with the columnar structure of the coatings.

The low density can be related with small grain size and with the correspondent increase of the volume

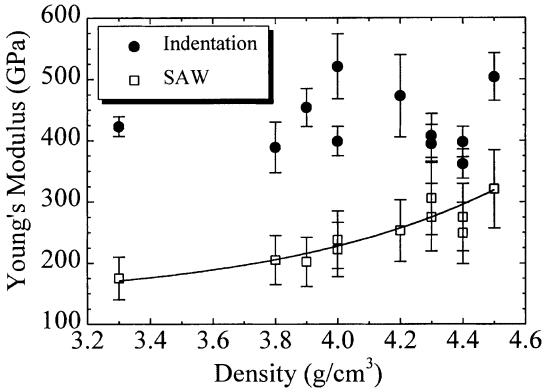

Fig. 6. Correlation between the Young's modulus of the (Ti,Al,Si)N coatings measured by both techniques (SAW and indentation) and density of the films.

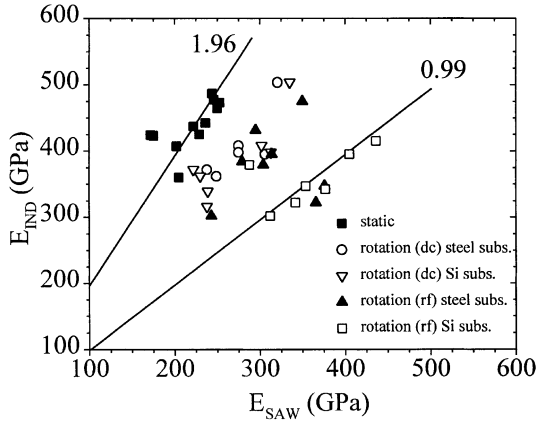

Fig. 7. Correlation between the Young's modulus of the (Ti,Al,Si)N coatings measured by SAW and indentation techniques.

fraction of grain boundaries [42], which agrees with broad diffraction peaks in some samples. However, other samples displayed narrow diffraction peaks, which means that low density should be related with the high degree of porosity. Although the low density values and consequent porosity could have some influence on elastic modulus measured by laser acoustic techniques, the microstructure should have some influence in low elastic modulus evidenced by the SAW technique. (Ti,Al,Si)N coatings deposited by rotation mode (rf supplied) on Si substrates, and simultaneously with those deposited on steel, showed an elastic modulus, measured by SAW, significantly higher than those of samples deposited on steel. Fig. 7 displays the correlation of elastic modulus determined by both techniques. The data show that different series have different correlations, which leads to a different behaviour. The slope of 0.99 for samples deposited on silicon by rotation mode (rf supplied) indicates a very good agreement between values obtained with both techniques. However, samples deposited on silicon in rotation mode (d.c. supplied), showed the same discrepancies in Young's modulus results as those deposited on steel.

The characteristics of high speed steel substrate, the density and Poisson ratio, were obtained from the literature and can be a source for a part of evidenced deviations by laser acoustic techniques. However, the distinct behaviour of samples prepared in different conditions seems to indicate that microstructure is the main source for those deviations. The best agreement appears with samples prepared in rotation mode (rf supplied), which are, in general, denser and have smaller grain size. The adhesion of the coatings can also influence the Young's modulus measured by SAW [43]. However, the films deposited on steel showed, in general, better adhesion than those deposited on silicon wafers.

4. Conclusions

The texture of different samples revealed the extreme importance of deposition parameters in the preparation of nanocomposite coatings, as exemplified by the presence of two different crystalline phases. These phases were already identified in (Ti,Si)N coatings.

Elastic moduli measured by SAW were found to be systematically lower than those obtained by indentation. The highest elastic modulus values measured by SAW technique were obtained with denser samples, which were prepared in rotation mode, showing some kind of correlation with the density of the samples. The best agreement between results from SAW and indentation techniques appeared with samples prepared in rotation mode (rf supplied), which are, in general, denser and have smaller grain size. The discrepancies between elastic modulus measured by both techniques suggest that SAW is sensitive to effective elastic modulus (depending on the effect of both matrix and defects), while indentation should be only sensitive to bulk elastic modulus (depending only on matrix).

Acknowledgements

The authors gratefully acknowledge the financial support from the FCT/MCT during the course of this scientific research under the project 32670/99 and pluri-annual program as well as financial support of the German/Portuguese DAAD/ICCTI institutions.

References

[1] M. Ohring, The Materials Science of Thin Films, Acad. Press, San Diego, 1992.
[2] D. Schneider, B. Schultrich, Surf. Coat. Technol. 98 (1998) 962.
[3] D. Schneider, M.D. Tucker, Thin Solid Films 290-291 (1996) 305.
[4] D. Schneider, T. Schwarz, H-P Buchkremer, D. Stöver, Thin Solid Films 224 (1993) 177.
[5] O.R. Shojaei, A. Karimi, Thin Solid Films 332 (1998) 202.
[6] M.D. Tran, J. Poublan, J.H. Dautzenberg, Thin Solid Films 308-309 (1997) 310.
[7] W.C. Oliver, G.M. Pharr, J. Mater. Res. 7 (1992) 1564.
[8] J. Mencik, M.V. Swain, J. Mater. Res. 10 (1995) 1491.
[9] C. Friedrich, G. Berg, E. Broszeit, C. Berger, Thin Solid Films 290-291 (1996) 216.
[10] N.X. Randall, R. Christoph, S. Droz, C. Julia-Schmutz, Thin Solid Films 290-291 (1996) 348.
[11] D. Schneider, Th. Schwarz, B. Schultrich, Thin Solid Films 219 (1992) 92.
[12] P. Hess, Appl. Surf. Sci. 106 (1996) 429.
[13] O. Knotek, W.D. Münz, T. Leyendecker, J. Vac. Sci. Technol. A 5 (1987) 2173.
[14] D. McIntyre, J.E. Greene, J.E. Sundgren, W.D. Münz, J. Appl. Phys. 67 (1990) 1542.
[15] H.A. Jehn, S. Hofmann, W.D. Münz, Thin Solid Films 153 (1987) 45.
[16] Y. Tanaka, T.M. Gur, M. Kelly, S.B. Hagstrom, T. Ikeda, Thin Solid Films 228 (1993) 238.
[17] F. Vaz, L. Rebouta, M. Andritschky, M.F. da Silva, J.C. Soares, J. Eur. Ceram. Soc. 17 (1997) 1971.
[18] F. Vaz, L. Rebouta, M. Andritschky, M.F. da Silva, J.C. Soares, Surf. Coat. Technol. 98 (1998) 912.
[19] P. Holubár, M. Jílek, M. Sima, Surf. Coat. Technol. 120-21 (1999) 184.
[20] S. Veprek, S. Reiprich, Thin Solid Films 268 (1995) 64.
[21] S. Veprek, Crit. Rev. J. Vac. Sci. Technol. A17 (1999) 2401.
[22] T. Hirai, S. Hayashi, J. Mater. Sci. 17 (1982) 1320.
[23] J.S. Reid, X. Sun, E. Kolawa, M.A. Nicolet, IEEE Electron. Device Lett. 15 (1994) 298.
[24] L. Shizhi, S. Yulong, P. Hongrui, Plasma Chem. Plasma Process. 12 (1992) 287.
[25] F. Vaz, L. Rebouta, S. Ramos, M.F. da Silva, J.C. Soares, Surf. Coat. Technol. 108-109 (1998) 236.
[26] M. Diserens, J. Patscheider, F. Lévy, Surf. Coat. Technol. 108-109 (1998) 241.
[27] I.N. Sneddon, Int. J. Eng. Sci. 3 (1965) 47.
[28] X. Jiang, M. Wang, K. Schmidt, E. Dunlop, J. Haupt, W. Gissler, J. Appl. Phys. 69 (1991) 3053.
[29] K.C. Tang, R.D. Arnell, Thin Solid Films 355-456 (1999) 263.
[30] E. Török, A.J. Perry, L. Chollet, W.D. Sproul, Thin Solid Films 154 (1987) 37.
[31] A.C. Trindade, A. Cavaleiro, J.V. Fernandes, J. Test. Eval. 22 (8) (1994) 365.
[32] G.M. Pharr, W.C. Oliver, MRS Bull. 17 (7) (1992) 28.
[33] S.R.J. Saunders, Surf. Eng. 9 (1993) 293.
[34] D. Schneider, H. Ollendorf, T. Schwarz, Appl. Phys. A223 (1995) 284.
[35] B. Auld, Acoustic Fields and Waves in Solids, Krieger Publ. Comp, Florida, 1973.
[36] H. Coufal, R. Grugier, P. Hess, A. Neubrand, J. Acous. Soc. Am. 92 (1992) 2980.
[37] G.W. Farnell, E.L. Adler, in: W.P. Mason, R.N. Thurston (Eds.), Physical Acoustics, Academic Press, New York, 1972 9, 35.
[38] D. Schneider, Th. Schwarz, H-J. Sceibe, M. Panzner, Thin Solid Films 295 (1997) 107.
[39] F. Vaz, L. Rebouta, B. Almeida et al., Surf. Coat. Technol. 120-121 (1999) 166.
[40] F. Vaz, L. Rebouta, P. Godeau et al., Surf. Coat. Technol. 133-134 (2000) 307.
[41] R.Y. Fillit, A.J. Perry, Surf. Coat. Technol. 36 (1988) 647.
[42] A.S. Edelstein, R.C. Cammarata, Nanomaterials: Syntheses, Properties and Applications, Institute of Physics Publ, Bristol, 1996.
[43] H. Ollendorf, D. Schneider, Surf. Coat. Technol. 113 (1999) 86.